Statistical theory of a self-seeded free electron laser with noise pedestal growth

Erik Hemsing,* Aliaksei Halavanau, and Zhen Zhang
SLAC National Accelerator Laboratory, Menlo Park, California 94025, USA

(Received 17 October 2019; published 2 January 2020)

We study the impact of a spectral noise pedestal on the statistical properties of a self-seeded free electron laser (FEL). The broad pedestal is assumed to come from self amplified spontaneous emission (SASE) in the second stage of the self-seeding system and is uncorrelated with the narrowband amplified seed. An analytic description is developed based on the statistical theory of a one-dimensional FEL in the high gain linear regime. The theory shows good agreement with experimental data, which show that the presence of a SASE background can have a strong impact on the statistical behavior of self-seeding systems.

DOI: 10.1103/PhysRevAccelBeams.23.010701

I. INTRODUCTION

Free electron lasers (FELs) use a beam of relativistic electrons to produce intense pulses of light down to hard x-ray wavelengths. Most short-wavelength single-pass FELs operate in SASE (self amplified spontaneous emission) mode, where density fluctuations from shot noise in the electron beam provide the input signal that is then amplified to saturation levels. Originating from noise, the output pulse of SASE FELs is also noisy and contains many uncorrelated temporal and frequency spikes within the $\sim 10^{-3}$ relative bandwidth [1,2].

To produce a narrower and cleaner output spectrum, self-seeded FELs rely on a spectral filter (such as a grating or crystal) to isolate a narrow region of SASE frequencies for amplification [3,4]. As such, self-seeded FELs are effectively split into two sections; the SASE stage that first provides the pulse to be spectrally filtered, and the seed stage that then amplifies the isolated narrowband ($\sim 10^{-4}$) seed pulse up to saturation. The pulse in the seed stage (i.e., the seed pulse) thus inherits some of the statistical properties of the upstream SASE pulse, depending on the linewidth of the spectral filter σ_m. Narrow linewidth filters (monochromators) select only a single coherent frequency spike from the SASE pulse, which has a shot-averaged bandwidth $\sigma_A \gg \sigma_m$. In this case, the seed has only a single temporal mode $M = 1/\sigma_\mathcal{E}^2$ which has 100% relative intensity fluctuations $\sigma_\mathcal{E}$ due to its noise origin [5]. Filters with wider linewidths that select multiple coherent spikes produce pulses that are overall more stable in integrated intensity, but come at the expense of a seed pulse that has multiple frequencies and thus more than one temporal mode.

In the seeded section, the seed pulse transmitted by the spectral filter must have enough power to overcome SASE growth in the second stage. Otherwise, the second stage will simply behave as a second SASE FEL starting from noise. Even for a strong seed, this can occur in different parts of the beam if the seed power varies strongly with time. For example, when the filter is wide enough to pass multiple temporal modes, there are low power regions of the pulse between coherent spikes that will not have enough seed power to overcome SASE growth in the seeded stage. The resulting FEL output spectrum will be a combination of the amplified narrow seed spikes and a broader SASE pedestal. This can be the case, for example, at the soft x-ray self-seeding system (SXRSS) at LCLS using electron beams longer than 10 fs [6,7]. The Fourier limited pulse length of the grating monochromator bandwidth is shorter than the electron beam, so the second stage is seeded by multiple temporal modes. The SASE growth impacts not just the spectrum, but the statistical behavior of the output. This is one motivation for the study presented here, where we extend previous work on the statistical properties of SASE FELs to include the effects of SASE growth during self-seeding.

The statistical properties of undulator and bend magnet radiation [8–11] and SASE FELs [12,13] have been studied previously. For a SASE FEL in the linear high-gain regime, a comprehensive treatment was provided by Saldin *et al.*, in [5]. Therein, the authors derive an expression for the statistical fluctuations of a spectrally filtered FEL output that depend on the SASE bandwidth, the filter bandwidth, and the electron beam bunch length. A one dimensional system is assumed in which the electron beam is long compared to the coherence length of the radiation.

*ehemsing@slac.stanford.edu

Here, we closely follow this description in extending the analysis to include the second amplification stage of both the main seed and an uncorrelated SASE background. We show that a SASE background will always increase the effective number of observed modes in the seed as characterized by the level of spectral energy fluctuations. The associated probability density function (PDF) of the combined SASE and seed output, here derived from a convolution of the individual gamma function distributions of the independent sources, skews the statistics toward the mean energy of the combined signal. Results of the analytic theory are then compared with experimental self-seeding data and are found to be in good agreement. This suggests that the seed and SASE in the second stage are indeed uncorrelated, and that the general framework serves to model the statistical behavior of the combined signal in the high-gain linear growth regime.

II. THEORY

In [5], it was shown that the electric field of a SASE FEL pulse just downstream of a spectral filter can be written as

$$E_s(\omega) = \sqrt{A_s} H_m(\omega) H_A(\omega) \tilde{I}_1(\omega), \tag{1}$$

where A_s is the intensity, $I_1(\omega)$ is the initial electron beam current spectrum, H_m is the filter transmission function, and H_A is the FEL Green's function,

$$|H_A(\omega)|^2 = \exp\left[-\frac{(\omega-\omega_0)^2}{2\sigma_A^2}\right], \tag{2}$$

with ω_0 the resonant frequency. The SASE pulse incident on the spectral filter has a frequency bandwidth

$$\sigma_A = 3\sqrt{\frac{2}{\sqrt{3}\hat{z}}}\rho\omega_0 \tag{3}$$

where $\hat{z} = 2\rho k_u z$ is the scaled distance of exponential growth along the undulator, $\lambda_u = 2\pi/k_u$ is the undulator period, and ρ is the FEL Pierce parameter [14]. Here we consider a filter with a Gaussian spectral profile, much like what one would have for the transverse electron beam size acting as its own exit slit

$$|H_m(\omega)|^2 = \exp\left[-\frac{(\omega-\omega_0)^2}{2\sigma_m^2}\right]. \tag{4}$$

The filter is centered about the maximum of the FEL gain bandwidth. From Eq. (1), it follows that the statistical properties of the field $E_s(\omega)$ are determined by the statistical properties of the initial current spectrum. Assuming this to be shot noise, $|E_s(\omega)|^2$ is distributed according to a negative exponential probability density function [5].

In self-seeding, $E_s(\omega)$ is the seed field that is placed back on the electron beam to be amplified in the second stage. The monochromator is typically inside a magnetic chicane that provides both a delay to temporally overlap the electron beam with $E_s(\omega)$, and also resets the electron beam current back to the shot noise level. We define this new current spectrum as $I_0(\omega)$, which is uncorrelated with $I_1(\omega)$. Thus the SASE in the first stage is uncorrelated with the SASE in the second stage. The resulting FEL field at the end of the second stage is the sum of two uncorrelated sources; a new SASE field $E_0(\omega)$ that grows starting from the beginning of the second stage, and the amplified seed field $E_1(\omega)$,

$$E(\omega) = E_0(\omega) + E_1(\omega). \tag{5}$$

In the spirit of Eq. (1), we explicitly identify the SASE field with intensity A_0, and the amplified seed field with intensity A_1 as

$$\begin{aligned} E_0(\omega) &= \sqrt{A_0} H_{A'}(\omega) \tilde{I}_0(\omega) \\ E_1(\omega) &= \sqrt{A_1} H_{A'}(\omega) H_m(\omega) H_A(\omega) \tilde{I}_1(\omega). \end{aligned} \tag{6}$$

The prime here identifies the second stage FEL Green's function $H_{A'}(\omega)$ which has the same form as in Eq. (2), but is differentiated from the first stage because it may have a different amplification length $\hat{z}'$ and thus a different bandwidth $\sigma_{A'}$ according to Eq. (3). We see that the amplified seed field $E_1(\omega)$ contains the memory of its origins in the first stage via $H_A(\omega)$ and $\tilde{I}_1(\omega)$, but, like the new SASE field $E_0(\omega)$, is amplified in the second stage according to the second stage FEL Green's function. Due to the linearity of the system, it is useful to note that the two FEL stages can be captured by a single Green's function, $H_{A'}(\omega, \hat{z}') H_A(\omega, \hat{z}) = H_A(\omega, \hat{z}' + \hat{z})$.

Defining the frequency-integrated total energy as $W = \int d\omega |E(\omega)|^2$, ensemble averaging over multiple pulses gives the following statistical quantities for the FEL pulse at the end of the second stage

$$\begin{aligned} \langle W \rangle &= \int d\omega \langle |E(\omega)|^2 \rangle, \\ \langle W^2 \rangle &= \int d\omega \int d\omega' \langle |E(\omega)|^2 |E(\omega')|^2 \rangle. \end{aligned} \tag{7}$$

The normalized variance, which characterizes the fluctuation levels, is then given by

$$\begin{aligned} \sigma_{\mathcal{E}}^2 &= \frac{\langle (W - \langle W \rangle)^2 \rangle}{\langle W \rangle^2} \\ &= \frac{\langle W_0^2 - \langle W_0 \rangle^2 \rangle + \langle W_1^2 - \langle W_1 \rangle^2 \rangle}{\langle W_0 + W_1 \rangle^2}. \end{aligned} \tag{8}$$

In the last step we have used the fact that the seed and the SASE pulses in the second stage are uncorrelated, $\langle W_0 \rangle \langle W_1 \rangle = \langle W_0 W_1 \rangle$.

We use the result from [5] that the first order frequency correlation in the current spectrum is $\langle I_0(\omega)I_0^*(\omega')\rangle = q^2NF(\omega-\omega')$ where $F(\omega)$ is the Fourier transform of the average temporal current profile and N is the number of electrons, and q is the electron charge. The second order correlation is $\langle|I_0(\omega)|^2|I_0(\omega')|^2\rangle = q^4N^2(1+F(\omega-\omega'))$. The same is true for I_1. Combining Eqs. (6) and (7) produces general expressions for the first and second moments of the SASE and seed energies in Eq. (8) (see the Appendix). We adopt finite integration bounds in the integral, $[\omega_0-\Delta\omega/2, \omega_0+\Delta\omega/2]$, to allow us to model a rectangular spectral filter at the end of the FEL (see Fig. 1). This can have an effect on the statistical behavior, as the window can isolate just the seed in a narrow bandwidth $\Delta\omega\sim\sigma_m$, or can broaden to include the SASE pedestal $\Delta\omega\sim\sigma_{A'}$. This approach bears resemblance to a previous experimental study that examined the statistical properties of SASE at hard x-rays [15].

We take the electron beam to have a rectangular temporal profile of duration T such that the first order frequency correlation for the current spectra is $|F(\omega-\omega')|^2 = \mathrm{sinc}^2[(\omega-\omega')T/2]$ [5]. The averaged energy quantities within the scaled integration bandwidth $\Delta\hat{\omega}=\Delta\omega T$ are then,

$$\begin{aligned}\langle W_0\rangle &= q^2N\sqrt{2\pi}\sigma_{A'}A_0\mathrm{erf}\left(\frac{\Delta\hat{\omega}}{2\sqrt{2}\hat{\sigma}_{A'}}\right)\\ \langle W_0^2\rangle &= \langle W_0\rangle^2[1+\sigma^2(\hat{\sigma}_{A'})]\\ \langle W_1\rangle &= q^2N\sqrt{2\pi}\sigma A_1\mathrm{erf}\left(\frac{\Delta\hat{\omega}}{2\sqrt{2}\hat{\sigma}}\right)\\ \langle W_1^2\rangle &= \langle W_1\rangle^2[1+\sigma^2(\hat{\sigma})]\end{aligned} \tag{9}$$

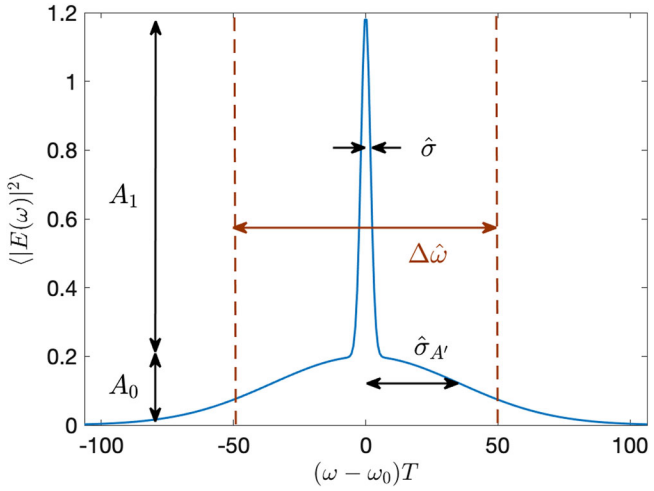

FIG. 1. Model of the averaged seeded output spectrum with uncorrelated broadband SASE pedestal. A_0 is the SASE intensity, A_1 the seed intensity, $\hat{\sigma}_{A'}$ is the scaled rms SASE bandwidth, $\hat{\sigma}$ the scaled rms seed bandwidth, and $\Delta\hat{\omega}$ is the window of integration.

where the scaled bandwidths are

$$\begin{aligned}\hat{\sigma}_m &= \sigma_m T, \qquad \hat{\sigma}_{A(')} = \sigma_{A(')}T,\\ \hat{\sigma}^2 &= \frac{\hat{\sigma}_m^2\hat{\sigma}_A^2\hat{\sigma}_{A'}^2}{\hat{\sigma}_m^2(\hat{\sigma}_A^2+\hat{\sigma}_{A'}^2)+\hat{\sigma}_A^2\hat{\sigma}_{A'}^2}.\end{aligned} \tag{10}$$

Note that the final bandwidth of the averaged seed spike is close to that of the monochromator $\hat{\sigma}\approx\hat{\sigma}_m$ when $\hat{\sigma}_m \ll \hat{\sigma}_A, \hat{\sigma}_{A'}$.

The normalized variance σ^2 of the seed and of the SASE in the second stage appears in Eq. (9) as a function of the individual bandwidths. Each can be calculated within the frequency window $\Delta\hat{\omega}$ of interest using the integral

$$\begin{aligned}\sigma^2(\hat{x}) = \frac{1}{2}\mathrm{erf}\left(\frac{\Delta\hat{\omega}}{2\sqrt{2}\hat{x}}\right)^{-2}\int_0^1(1-\xi)e^{-(\hat{x}\xi)^2}\\ \times\left[\mathrm{erf}\left(\frac{\Delta\hat{\omega}-2i\hat{x}^2\xi}{2\sqrt{2}\hat{x}}\right)+\mathrm{erf}\left(\frac{\Delta\hat{\omega}+2i\hat{x}^2\xi}{2\sqrt{2}\hat{x}}\right)\right]^2 d\xi,\end{aligned} \tag{11}$$

where $\hat{x}=\hat{\sigma}$ or $\hat{\sigma}_{A'}$. This term gives the level of fluctuations within the window $\Delta\hat{\omega}$, and comes from integration over $|F(\omega-\omega')|^2$. It characterizes the extent to which the details of the average beam distribution contribute to the fluctuations (see Appendix). As shown in Fig. 2, the normalized variance has the following general behavior, depending on the window $\Delta\hat{\omega}$:

$$\sigma^2(\hat{x}) \approx \begin{cases}1, & \text{for } \Delta\hat{\omega}<1\\ 2\pi/\Delta\hat{\omega}, & \text{for } 1\ll\Delta\hat{\omega}\le\hat{x}\\ \sqrt{\pi}/\hat{x} & \text{for } 1\ll\hat{x}\ll\Delta\hat{\omega}.\end{cases} \tag{12}$$

For example, with SASE alone, the fluctuations are given by $\sigma^2(\hat{\sigma}_{A'})$.

Inserting the second moments in Eq. (9) into the total normalized variance in Eq. (8), we obtain an expression for

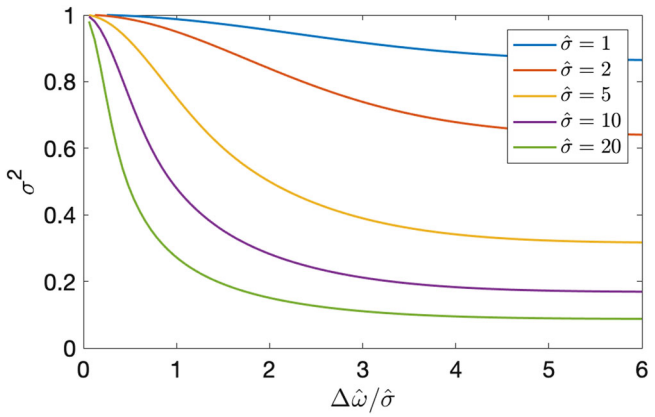

FIG. 2. Variance σ^2 in Eq. (11) as a function of window $\Delta\hat{\omega}$ for different bandwidths $\hat{\sigma}$.

an effective total number of modes when the seed and SASE contribution are both included [16],

$$M = \frac{1}{\sigma_{\mathcal{E}}^2} = \frac{\langle W_0 + W_1\rangle^2}{\langle W_0\rangle^2/M_0 + \langle W_1\rangle^2/M_1}. \tag{13}$$

We can identify the modes associated with the fluctuations of the individual SASE and seeded spectra

$$M_0 = \frac{1}{\sigma^2(\hat{\sigma}_{A'})}, \qquad M_1 = \frac{1}{\sigma^2(\hat{\sigma})}. \tag{14}$$

We see that, if the SASE component vanishes, $M = M_1$ and $\sigma_{\mathcal{E}}^2 = \sigma^2(\hat{\sigma})$.

Figure 3 shows how the total number of modes in Eq. (13) increases with the mean SASE energy. The behavior shown is true for any windowed bandwidth $\Delta\hat{\omega}$, so it can be seen how the presence of SASE impacts the statistics of the total signal inside a narrow window within the seed (when $M_0/M_1 \approx 1$), or over the whole spectrum ($M_0/M_1 \gg 1$). In either case, if the relative SASE energy within the window is very small ($\langle W_0\rangle/\langle W_1\rangle \ll 1$), M increases approximately linearly with $\langle W_0\rangle/\langle W_1\rangle$.

From Eqs. (12) and (14) the number of individual SASE and seed modes are determined by either the window bandwidth or the intrinsic bandwidth of each respective signal. In the $\Delta\hat{\omega} \to \infty$ limit, one obtains the independent results $M_0 = \hat{\sigma}_A/\sqrt{\pi}$ and $M_1 = \hat{\sigma}/\sqrt{\pi}$ that can be retrieved from Ref. [5]. However, when both sources are present, the statistical behavior of the system changes according to Eq. (13). Notably, when the window is smaller than the spectral interval of coherence, $\Delta\hat{\omega} < 1$ then M_0, $M_1 = 1$ and

$$M = \frac{(A_0 + A_1)^2}{A_0^2 + A_1^2} \quad \text{for} \quad \Delta\hat{\omega} < 1. \tag{15}$$

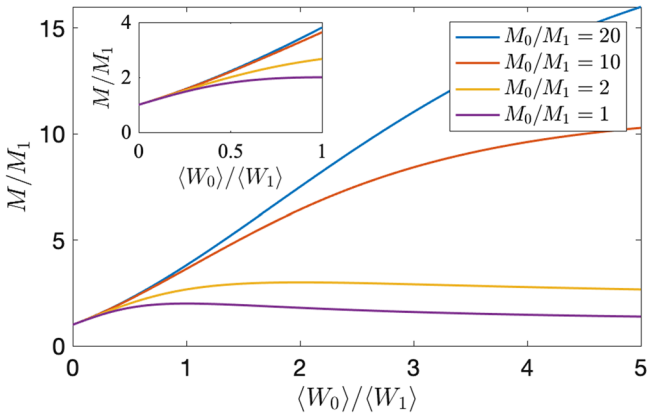

FIG. 3. Total mode number in Eq. (13) relative to the number of seed modes M_1 as a function of the relative SASE energy. As the SASE energy grows compared to the seed, the number of modes also grows until $M \approx M_0$.

We see that $1 \le M \le 2$. It is never unity unless either source vanishes, so the presence of a SASE background will always make it appear that there is more than one mode in the seed, even for narrow integration bandwidths. We note that written in the form $M = \frac{2}{1+P^2}$ with the definition $P = \frac{A_0 - A_1}{A_0 + A_1}$, it bears a striking resemblance to that of a partially polarized wave with P the degree of polarization [17].

The behavior of the total number of modes as a function of $\Delta\hat{\omega}$ is shown in Fig. 4 for different SASE levels. When only the amplified seed is present (no SASE pedestal) the number of modes is small, as defined primarily by the narrow monochromator bandwidth $\hat{\sigma} \approx \hat{\sigma}_m$. When only SASE is present (e.g., if the seed is blocked) the number of modes is large due to the large SASE bandwidth $\hat{\sigma}_{A'}$. Because the SASE bandwidth is much larger than the seed bandwidth, even a small relative SASE pedestal amplitude $A_0/A_1 \ll 1$ can have a strong effect on the statistical behavior of the amplified seed, especially when integrating over the whole spectrum ($\hat{\sigma}_{A'} \ll \Delta\hat{\omega}$). For example, for the parameters used in Fig. 4, when the average SASE spectral intensity peak is only 5% that of the seed, it still doubles the effective number of modes measured by the total pulse energy. This is because, as given in Eq. (9), the integrated energy in the broadband SASE component can be significant. Therefore, in the presence of a SASE pedestal, the statistical properties of a self-seeded FEL can depend strongly on the window bandwidth, and thus may inform the use of a post-FEL monochromator.

A. Probability density function

Clearly the SASE pedestal alters the spectrum and the level of fluctuations in the self-seeded signal. Thus it modifies the probability distribution of radiation energy. Because the SASE and seed signals are independent, the probability density of their sum is the convolution of their probability densities [17]. We assume that the seed signal

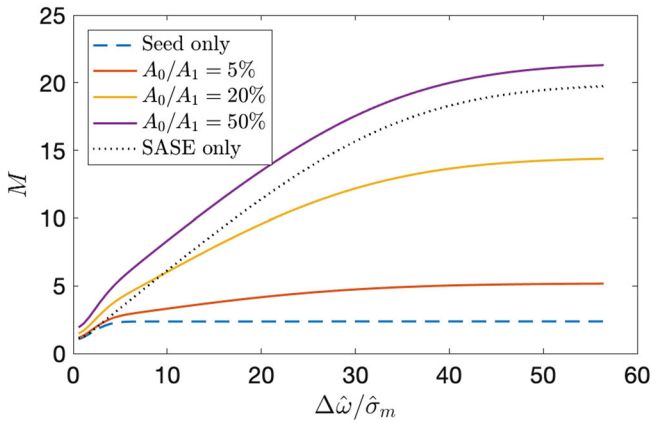

FIG. 4. Total modes versus window bandwidth for varying SASE pedestal amplitude. $\hat{\sigma}_m = 2\sqrt{\pi}$ and $\hat{\sigma}_A = 20\sqrt{\pi}$.

and the SASE signal each obey their own gamma probability distribution,

$$p_{M_i}(W_i) = \frac{M_i^{M_i}}{\langle W_i\rangle \Gamma(M_i)} \left(\frac{W_i}{\langle W_i\rangle}\right)^{M_i-1} \exp\left(-M_i \frac{W_i}{\langle W_i\rangle}\right). \tag{16}$$

FEL radiation has been measured to exhibit this distribution in the linear regime at multiple FEL facilities operating at different photon energies, e.g., in [10,15,18–23]. We also note that in the limit of a very large M, Eq. (16) asymptotically becomes Gaussian.

The probability density function (PDF) of the sum signal is given by the convolution,

$$p_M(W) = \int_0^W p_{M_1}(W-x) p_{M_0}(x) dx. \tag{17}$$

The limits of integration are set by bounds on the individual PDFs, namely $p_{M_i}(x) = 0$ for $x < 0$. The total PDF is then

$$p_M(W) = \frac{W^{M_0+M_1-1}}{\Gamma(M_0+M_1)} \left(\frac{M_0}{\langle W_0\rangle}\right)^{M_0} \left(\frac{M_1}{\langle W_1\rangle}\right)^{M_1} \times e^{-M_1\frac{W}{\langle W_1\rangle}} {}_1F_1\left[M_0, M_0+M_1, \left(\frac{M_1}{\langle W_1\rangle} - \frac{M_0}{\langle W_0\rangle}\right) W\right]. \tag{18}$$

Here ${}_1F_1$ is the Kummer confluent hypergeometric function. One can confirm that this total PDF returns the proper values for the mean of W

$$\langle W\rangle = \int_0^\infty W p_M(W) dW = \langle W_0 + W_1\rangle, \tag{19}$$

and the normalized variance,

$$\sigma_{\mathcal{E}}^2 = \int_0^\infty \frac{(W-\langle W\rangle)^2}{\langle W\rangle^2} p_M(W) dW = \frac{1}{M}, \tag{20}$$

where M is defined in Eq. (13). In fact, the nth moment of W can be found from $\langle W^n\rangle = \frac{d^n\varphi(t)}{i^n dt^n}|_{t=0}$ where $\varphi(t) = \langle \exp(itW)\rangle = (1 - it\langle W_0\rangle/M_0)^{-M_0}(1 - it\langle W_1\rangle/M_1)^{-M_1}$ is the total characteristic function of the sum signal. It is the Fourier transform of the total PDF and, by the convolution theorem, is the product of the characteristic functions for the individual PDFs in (16).

In the limit that SASE vanishes $\langle W_0\rangle = 0$, the total PDF in (18) returns to a Gamma probability density function for the seed signal with M_1 modes and mean $\langle W_1\rangle$. In the presence of a finite SASE contribution, the total PDF becomes skewed. Examples are shown in Fig. 5. The SASE pedestal shifts the peak of the PDF curve toward the mean.

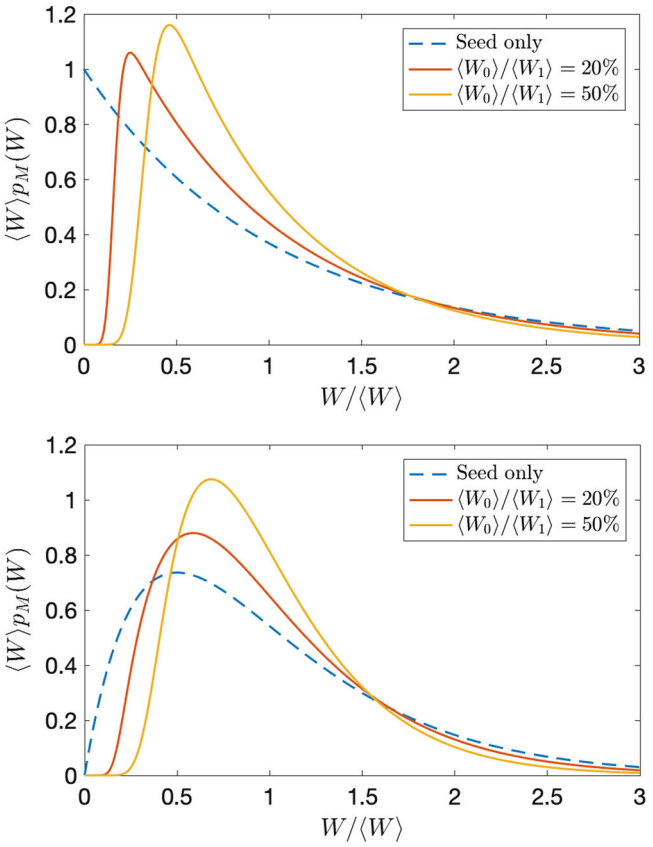

FIG. 5. Total PDF with $M_0 = 20$ SASE modes and $M_1 = 1$ seed mode (top) and $M_1 = 2$ seed modes (bottom). The SASE background increases the likelihood of the radiation energy for a given shot occurring near the mean, and reduces the likelihood of small signals.

It also sharply reduces the probability of measuring small signals near $W = 0$.

III. COMPARISON WITH EXPERIMENT

The analytic model can be compared directly with experimental data obtained from recent soft x-ray self-seeding (SXRSS) experiments at LCLS [7,16]. Experiments were performed at a photon energy of 1 keV, and the averaged spectral output is shown in Fig. 6. Spectral measurements over 2335 independent shots were recorded at a fixed position corresponding to a scaled length $\hat{z}' =$ 6–7 downstream of the SXRSS system where there is near full transverse coherence [24,25]. The SXRSS system itself is at a similar length through the first stage of undulators, so the SASE bandwidths in each stage are approximately equal ($\hat{\sigma}_A = \hat{\sigma}_{A'}$). Because saturation occurs near $\hat{z} = 9$, the lengths of both stages are within the high gain linear mode of FEL operation where the present theory is presumed applicable. Additional details of the SXRSS system and experimental data can be found in [6,7,16].

From Fig. 6, the main seed line sits atop a small SASE pedestal from the second stage, which can be measured

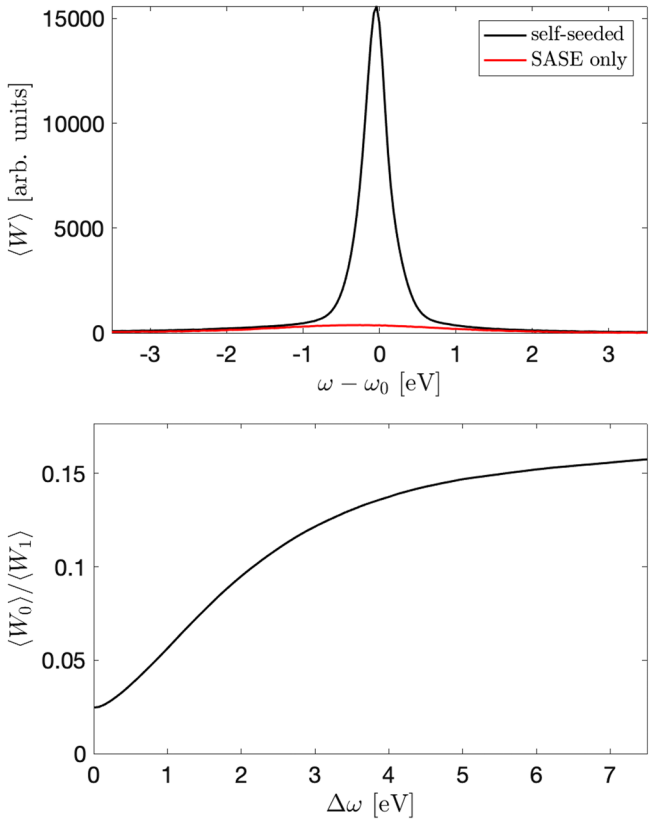

FIG. 6. Top: Averaged measured self-seeding spectrum at LCLS U15 undulator. With the seed blocked, the SASE from the second stage can be measured directly, and used to compute the contribution from the seed alone. Bottom: Measured average ratio of SASE to seeded energy versus bandwidth.

independently by blocking the seed in the SXRSS system. The laser heater was set to 30 μJ, which is large enough to strongly suppress the microbunching-driven pedestal. The relative pure SASE amplitude is $A_0/A_1 = 2.4\%$, and the SASE bandwidth is $\sigma_{A'} = 1.15$ eV using a Gaussian fit. The design FWHM bandwidth of the grating monochromator and x-ray optics system in the SXRSS is 200 meV, corresponding to an intrinsic rms bandwidth of the seed of $\sigma_m = 85$ meV. Due to the roughly 250 meV point-spread function of the spectrometer [7] and some spectral broadening from resistive wall wakefields in the undulator chambers [26], this narrow width cannot be fully resolved in the measured data. The relative energy ratio of the SASE to the seed $\langle W_0 \rangle / \langle W_1 \rangle$ as a function of $\Delta\omega$ can also be obtained from the averaged spectra, first by the measure of SASE contribution alone ($\langle W_0 \rangle$) and then computed for the seed using the total signal $\langle W \rangle = \langle W_0 \rangle + \langle W_1 \rangle$ from Eq. (20). This ratio is shown in the lower plot of Fig. 6.

Using these quantities from the averaged spectra, the total number of modes M can be calculated from the theory using Eq. (13) and assuming an electron beam duration of $T = 55$ fs. The result is plotted in Fig. 7. Also plotted is the total number of modes calculated directly from fluctuations of the multishot spectra. Good agreement is found in the

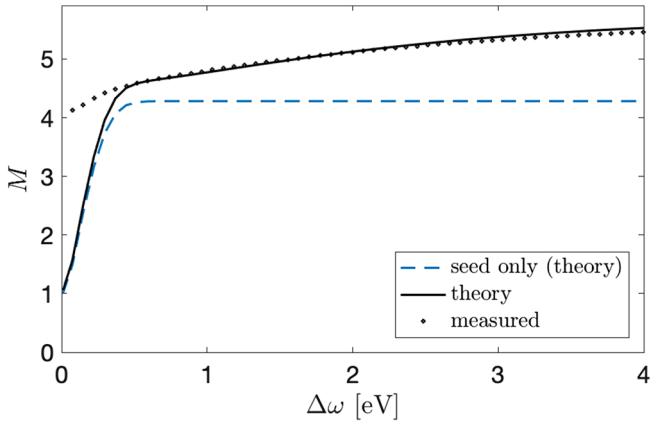

FIG. 7. Total measured number of modes versus bandwidth. The black line is calculated from the expression in Eq. (13), and the dotted line is directly from measured fluctuations.

region where the spectral window is large $\Delta\omega \gg \sigma_m$ and the broadband SASE energy drives up the mode number by reducing the integrated fluctuations. Both approaches predict $M = 4$–5 modes in the seed, which is consistent with the beam length compared to the short 9 fs Fourier limited pulse length set by the monochromator bandwidth. We note that there is some uncertainty both in the true monochromator bandwidth σ_m and in the effective lasing core of the beam T, but that the statistical behavior for $\Delta\omega \gg \sigma_m$ is unaffected for a reasonable range of alternate values if $\sigma_m T = \hat{\sigma}_m$ remains fixed. Within small measurement windows ($\Delta\omega \to 0$) the true σ_m could be determined in principle with better spectral resolution. We see that the lack of resolution in this range also precludes determination of the statistics from the fluctuations of the multi-shot spectra.

Figure 8 shows the histograms of the normalized integrated spectral intensity of the seed over the full seed bandwidth ($\Delta\omega = 1.1$ eV) and over the full SASE bandwidth ($\Delta\omega = 7.5$ eV). Also shown are the gamma PDFs for a pure seed with $M = 4.3$ modes, and the total PDFs from Eq. (18). The total PDFs are calculated using the measured energy ratio $\langle W_0 \rangle / \langle W_1 \rangle$ and mode numbers M_0 and M_1 [calculated from the bandwidths σ and $\sigma_{A'}$ and Eq. (14)] within each window of integration. Results for the narrow integration window (top plot) show that the statistics predicted by the total PDF and the Gamma PDF are similar, and that they both match well with the measured data for a seed that contains $M_1 = 4.3$ modes. The similarity between the two PDFs is to be expected, as the fractional SASE energy within the seed is small. For the larger integration window, however, the fractional SASE energy becomes large enough to distinguish the two curves. Shown in the bottom plot, the total PDF predicts a higher probability of shots with energy near the mean value, and a slight reduction in the number of shots with less energy. This is confirmed empirically by the data, which appears to better follow the statistics of the total PDF rather than a simple gamma distribution. These results indicate that, in practice,

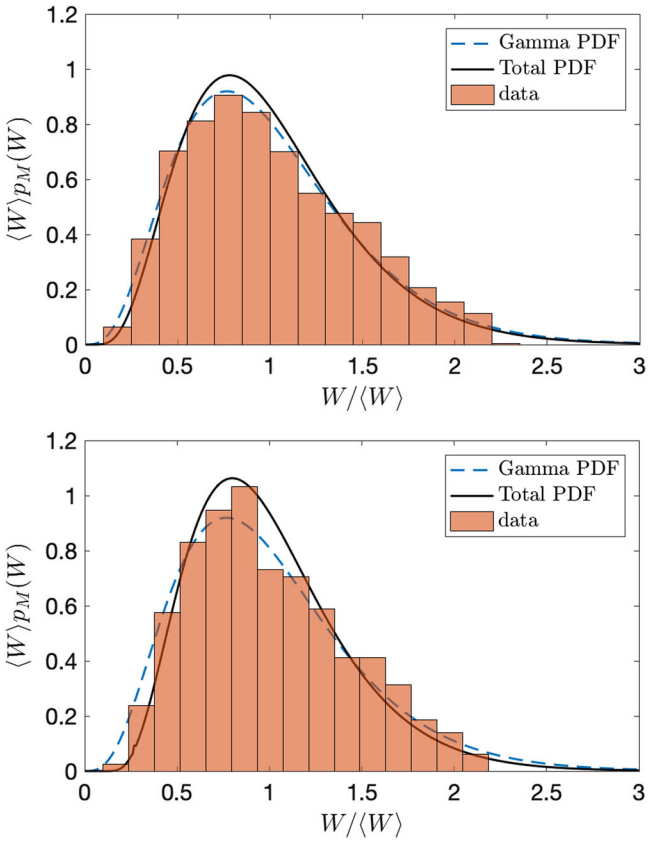

FIG. 8. Histograms of the measured SXRSS spectrum from LCLS within a $\Delta\omega = 1.1$ eV window (top) and a $\Delta\omega = 7.5$ eV window (bottom). The dashed line denotes a gamma PDF [Eq. (16)] of a pure seed (no SASE background) with $M = M_1 = 4.3$, as given by FIG. 7. The solid line is the prediction from the total PDF in Eq. (18) that includes the SASE contribution. Within the narrow window (top) the measured SASE portion is small ($\langle W_0\rangle/\langle W_1\rangle = 6.4\%$, $M_0 = 16$), so the two PDFs are nearly identical. Within the larger window, however, the larger SASE contribution ($\langle W_0\rangle/\langle W_1\rangle = 15.7\%$, $M_0 = 52$) shifts the statistics slightly. In this case the total PDF in Eq. (18) is qualitatively a better fit to the SXRSS data.

the SASE component of the self-seeding signal should be incorporated in evaluating the statistical properties of the FEL, especially if no postmonochromator is used to select a narrowed region of the spectrum.

IV. CONCLUSION

We have analyzed the statistical properties of a self-seeded FEL in the presence of SASE growth in the second stage. Assuming the two sources are uncorrelated, we derive an expression for the effective total number of modes in the combined signal which depends on the number of modes and average energy of each source. The SASE background is shown to always increase the number of modes in the seed, particularly when the full spectrum is included. Experimentally, it may therefore be advantageous to aperture the spectral window to limit the number of modes, especially if the SASE background is appreciable. A probability density function for the combined signal is then derived and matched against the statistics from SXRSS experiments, showing good agreement. Together, these results suggest that the presented framework is a reasonable model for the statistical behavior of self-seeded FEL in the presence of SASE noise.

ACKNOWLEDGMENTS

We thank W. M. Fawley, A. A. Lutman, G. Marcus, C. Pellegrini, E. Schneidmiller, and G. Stupakov for helpful conversations. This work was supported by U.S. Department of Energy Contract No. DE-AC02-76SF00515 and Award No. 2017-SLAC-100382.

APPENDIX

The ensemble-averaged energy moments for the SASE and seed in the total variance [Eq. (8)] are found by inserting the expressions for the individual fields [Eq. (6)] into the integrals in Eq. (7). We obtain

$$\begin{aligned}
\langle W_0\rangle &= q^2 N A_0 \int d\omega |H_{A'}(\omega)|^2,\\
\langle W_1\rangle &= q^2 N A_1 \int d\omega |H_{A'}(\omega)|^2 |H_A(\omega)|^2 |H_m(\omega)|^2,\\
\langle W_0^2\rangle &= q^4 N^2 A_0^2 \int d\omega \int d\omega' |H_{A'}(\omega)|^2 |H_{A'}(\omega')|^2 (1 + |F(\omega-\omega')|^2),\\
\langle W_1^2\rangle &= q^4 N^2 A_1^2 \int d\omega \int d\omega' |H_{A'}(\omega)|^2 |H_{A'}(\omega')|^2 |H_A(\omega)|^2 |H_A(\omega')|^2 |H_m(\omega)|^2 |H_m(\omega')|^2 (1 + |F(\omega-\omega')|^2). \qquad \text{(A1)}
\end{aligned}$$

Using a flattop (rectangular) beam profile, the frequency correlation is

$$|F(\omega-\omega')|^2 = \mathrm{sinc}^2[(\omega-\omega')T/2]. \tag{A2}$$

Combined, we obtain the expressions in Eq. (9). Within the expressions for $\langle W_0^2\rangle$ and $\langle W_1^2\rangle$ is the normalized variance σ^2, given by the integral in Eq. (11). This integral is the result of the Fourier transform

$$\mathrm{sinc}^2(\omega T/2) = \int \mathrm{tri}(\xi) e^{i\omega T\xi} d\xi \tag{A3}$$

where the triangle function $\mathrm{tri}(\xi) = 1-|\xi|$ for $|\xi|<1$, and $\mathrm{tri}(\xi)=0$ otherwise.

When $\Delta\hat{\omega}\to\infty$, Eq. (11) becomes,

$$\sigma^2(\hat{\sigma}) = \frac{\sqrt{\pi}\hat{\sigma}\mathrm{erf}(\hat{\sigma}) + e^{-\hat{\sigma}^2} - 1}{\hat{\sigma}^2} \tag{A4}$$

which approaches $\sqrt{\pi}/\hat{\sigma}$ for $\hat{\sigma}\gg 1$.

[1] K.-J. Kim, An analysis of self-amplified spontaneous emission, Nucl. Instrum. Methods Phys. Res., Sect. A **250**, 396 (1986).

[2] J.-M. Wang and L.-H. Yu, A transient analysis of a bunched beam free electron laser, Nucl. Instrum. Methods Phys. Res., Sect. A **250**, 484 (1986).

[3] J. Feldhaus, E. L. Saldin, J. R. Schneider, E. A. Schneidmiller, and M. V. Yurkov, Possible application of X-ray optical elements for reducing the spectral bandwidth of an X-ray SASE FEL, Nucl. Instrum. Methods Phys. Res., Sect. A **393**, 162 (1997).

[4] G. Geloni, V. Kocharyan, and E. Saldin, A novel self-seeding scheme for hard X-ray FELs, J. Mod. Opt. **58**, 1391 (2011).

[5] E. L. Saldin, E. A. Schneidmiller, and M. V. Yurkov, Statistical properties of radiation from VUV and X-ray free electron laser, Opt. Commun. **148**, 383 (1998).

[6] D. Ratner, R. Abela, J. Amann, C. Behrens, D. Bohler, G. Bouchard, C. Bostedt, M. Boyes, K. Chow, D. Cocco *et al.*, Experimental Demonstration of a Soft X-Ray Self-Seeded Free-Electron Laser, Phys. Rev. Lett. **114**, 054801 (2015).

[7] G. Marcus, W. M. Fawley, D. Bohler, Y. Ding, Y. Feng, E. Hemsing, Z. Huang, J. Krzywinski, A. Lutman, and D. Ratner, Experimental observations of seed growth and accompanying pedestal contamination in a self-seeded, soft x-ray free-electron laser, Phys. Rev. Accel. Beams **22**, 080702 (2019).

[8] M. C. Teich, T. Tanabe, T. C. Marshall, and J. Galayda, Statistical Properties of Wiggler and Bending-Magnet Radiation from the Brookhaven Vacuum-Ultraviolet Electron Storage Ring, Phys. Rev. Lett. **65**, 3393 (1990).

[9] M. S. Zolotorev and G. V. Stupakov, Report No. SLAC-PUB-7132, 1996.

[10] P. Catravas, W. Leemans, J. Wurtele, M. Zolotorev, M. Babzien, I. Ben-Zvi, Z. Segalov, X.-J. Wang, and V. Yakimenko, Measurement of Electron-Beam Bunch Length and Emittance Using Shot-Noise-Driven Fluctuations in Incoherent Radiation, Phys. Rev. Lett. **82**, 5261 (1999).

[11] F. Sannibale, G. V. Stupakov, M. S. Zolotorev, D. Filippetto, and L. Jägerhofer, Absolute bunch length measurements by incoherent radiation fluctuation analysis, Phys. Rev. Accel. Beams **12**, 032801 (2009).

[12] R. Bonifacio, L. De Salvo, P. Pierini, N. Piovella, and C. Pellegrini, Spectrum, Temporal Structure, and Fluctuations in a High-Gain Free-Electron Laser Starting from Noise, Phys. Rev. Lett. **73**, 70 (1994).

[13] K.-J. Kim, Start-up noise in 3-D self-amplified spontaneous emission, Nucl. Instrum. Methods Phys. Res., Sect. A **393**, 167 (1997), free Electron Lasers 1996.

[14] R. Bonifacio, C. Pellegrini, and L. Narducci, Collective instabilities and high-gain regime in a free electron laser, Opt. Commun. **50**, 373 (1984).

[15] A. Lutman, Z. Huang, J. Krzywinski, J. Wu, D. Zhu, and Y. Feng, in *Advances in X-ray Free-Electron Lasers Instrumentation IV*, Vol. 10237, edited by T. Tschentscher and L. Patthey, International Society for Optics and Photonics (SPIE, Prague, 2017) pp. 51–60.

[16] Z. Zhang, G. Marcus, E. Hemsing, W. M. Fawley, Z. Huang, and A. Lutman, Statistical analysis of a self-seeded x-ray free-electron laser in the presence of the micro-bunching instability, Phys. Rev. Accel. Beams (to be published).

[17] J. Goodman, *Statistical Optics*, *Wiley Series in Pure and Applied Optics* (Wiley, New York, 2000).

[18] M. Hogan, C. Pellegrini, J. Rosenzweig, G. Travish, A. Varfolomeev, S. Anderson, K. Bishofberger, P. Frigola, A. Murokh, N. Osmanov, S. Reiche, and A. Tremaine, Measurements of High Gain and Intensity Fluctuations in a Self-Amplified, Spontaneous-Emission Free-Electron Laser, Phys. Rev. Lett. **80**, 289 (1998).

[19] A. Murokh *et al.*, Properties of the ultrashort gain length, self-amplified spontaneous emission free-electron laser in the linear regime and saturation, Phys. Rev. E **67**, 066501 (2003).

[20] A. Tremaine, P. Frigola, A. Murokh, C. Pellegrini, S. Reiche, J. Rosenzweig, M. Babzien, I. Ben-Zvi, E. Johnson, R. Malone, G. Rakowsky, J. Skaritka, X. J. Wang, and V. Yakimenko, in *Proceedings of the 19th Particle Accelerator Conference, Chicago, IL, 2001* (IEEE, Piscataway, NJ, 2001), Vol. 4, pp. 2760–2762.

[21] M. Yurkov, Statistical properties of SASE FEL radiation: Experimental results from the VUV FEL at the TESLA test facility at DESY, Nucl. Instrum. Methods Phys. Res., Sect. A **483**, 51 (2002).

[22] A. Singer, F. Sorgenfrei, A. P. Mancuso, N. Gerasimova, O. M. Yefanov, J. Gulden, T. Gorniak, T. Senkbeil, A. Sakdinawat, Y. Liu, D. Attwood, S. Dziarzhytski, D. D. Mai, R. Treusch, E. Weckert, T. Salditt, A. Rosenhahn, W. Wurth, and I. A. Vartanyants, Spatial and temporal coherence properties of single free-electron laser pulses, Opt. Express **20**, 17480 (2012).

[23] O. Y. Gorobtsov, G. Mercurio, F. Capotondi, P. Skopintsev, S. Lazarev, I. A. Zaluzhnyy, M. B. Danailov, M. Dell'

Angela, M. Manfredda, E. Pedersoli, L. Giannessi, M. Kiskinova, K. C. Prince, W. Wurth, and I. A. Vartanyants, Seeded X-ray free-electron laser generating radiation with laser statistical properties, Nat. Commun. **9**, 4498 (2018).

[24] Y. Ding, Z. Huang, S. A. Ocko *et al.*, in *Proceedings of the 32nd Free Electron Laser Conference, Malmö, Sweden* (Max-lab, Sweden, 2010).

[25] I. A. Vartanyants *et al.*, Coherence Properties of Individual Femtosecond Pulses of an X-Ray Free-Electron Laser, Phys. Rev. Lett. **107**, 144801 (2011).

[26] E. Hemsing, G. Marcus, W. M. Fawley, R. W. Schoenlein, R. Coffee, G. Dakovski, J. Hastings, Z. Huang, D. Ratner, T. Raubenheimer, and G. Penn, Soft x-ray seeding studies for the SLAC Linac Coherent Light Source II, Phys. Rev. Accel. Beams **22**, 110701 (2019).